

Angle-resolved photoemission spectra, electronic structure, and spin-dependent scattering in $\text{Ni}_{1-x}\text{Fe}_x$ Permalloys

P. E. Mijnders

*Department of Physics, Northeastern University, Boston, Massachusetts 02115
and Interfaculty Reactor Institute, Delft University of Technology, Delft, The Netherlands*

S. Sahrakorpi and M. Lindroos

*Institute of Physics, Tampere University of Technology, 33101 Tampere, Finland
and Department of Physics, Northeastern University, Boston, Massachusetts 02115*

A. Bansil

Department of Physics, Northeastern University, Boston, Massachusetts 02115

(Received 28 June 2001; published 22 January 2002)

We present the all-electron charge and spin self-consistent electronic structure of $\text{Ni}_{1-x}\text{Fe}_x$ Permalloys for a range of Fe concentrations, using the first-principles Korringa-Kohn-Rostoker coherent potential approximation (KKR-CPA) scheme to treat disorder and the local spin density approximation to incorporate exchange-correlation effects. Recent high-resolution angle-resolved photoemission spectroscopy (ARPES) experiments on $\text{Ni}_{0.90}\text{Fe}_{0.10}$ and $\text{Ni}_{0.80}\text{Fe}_{0.20}$ Permalloys are analyzed in terms of the spectral density function, $A_B(\mathbf{k}_{\parallel}, \mathbf{k}_{\perp} = \mathbf{0}, E_F)$, computed from the KKR-CPA Green function for \mathbf{k}_{\parallel} values varying along the Γ - K direction in the Brillouin zone. The widths of the majority as well as the minority spin peaks in the theoretical spectra are in excellent accord with the corresponding ARPES results in all cases, suggesting that spin-dependent disorder scattering constitutes the main scattering mechanism for the carriers in the Permalloys. Majority spin states of Ni are virtually undamped by the Fe impurities, while the minority spins at the Fermi energy (E_F) are heavily damped. The nature of the Ni and Fe potentials in the Permalloys is explored in detail. The effective disorder parameter in the alloy is found to be strongly dependent on the energy, momentum, spin, and symmetry of the specific states involved. The evolution of the electronic states on the Ni and Fe sites as a function of Fe concentration is discussed. The magnetic moments on Ni as well as on Fe are found to remain essentially unchanged with increasing Fe content.

DOI: 10.1103/PhysRevB.65.075106

PACS number(s): 79.60.-i, 72.25.Ba, 71.23.-k

I. INTRODUCTION

Recent years have seen a rapidly growing interest in the field of magnetoelectronics.¹ Physical phenomena such as anisotropic or giant magnetoresistance, which allow the control of electronic spin currents through magnetically doped nanometer structures by an external magnetic field, while interesting in their own right, are also of great technological interest.^{2,3} Among the materials playing a role in these nanostructures, Permalloys (high-permeability alloys of Ni and Fe) take an important place. Permalloy/Cu/Co films showing a giant magnetoresistance (GMR) effect act as spin valves in which the electrical resistivity is low or high depending on the orientation of an external magnetic field. The advantage of using Permalloy in these nanostructures lies in the fact that the magnetostriction in $\text{Ni}_{0.80}\text{Fe}_{0.20}$ vanishes. This prevents the strain due to lattice constant mismatch in the nanostructure from magnetizing the material. Bulk Permalloy also shows (relatively small) anisotropic magnetoresistivity (AMR) which is used in reading heads for hard disks.

In order to understand the operation of either thin-film or bulk devices an understanding of the electronic structure and transport properties of the materials involved is essential. Much of the existing experimental work has concentrated on measuring the spin-dependent resistivities or mean free paths of majority and minority spin electrons in various materials.⁴⁻⁸ Accordingly, theoretical studies have focused

on transport properties of the bulk systems and how these are affected by the presence of relevant interfaces.⁹⁻¹¹ However, the interpretation of transport phenomena is intrinsically complicated by the fact that they encompass the behavior of *all* the electrons at the Fermi energy (E_F). With recent advances in synchrotron light sources and detector technology, high-resolution angle-resolved photoemission spectroscopy (ARPES) now offers the exciting possibility of investigating the character of *individual* \mathbf{k} states in magnetic materials.^{12,13} In particular, Ref. 13 has presented ARPES measurements from high-quality samples of $\text{Ni}_{0.90}\text{Fe}_{0.10}$ and $\text{Ni}_{0.80}\text{Fe}_{0.20}$ for specific majority and minority spin states at E_F for \mathbf{k}_{\parallel} values lying along the Γ - K direction in the Brillouin zone (BZ).

The preceding considerations provide a strong motivation for undertaking a study such as the present one which attempts to make direct contact between the aforementioned ARPES experiments on Permalloys and the corresponding predictions of the first-principles framework of the alloy theory. We confront the computed widths of the spectral density obtained from the self-consistent parameter-free Korringa-Kohn-Rostoker coherent-potential-approximation local-spin-density (KKR-CPA-LSD) Green function¹⁴⁻¹⁹ with the ARPES results and find an excellent level of accord between theory and experiment with respect to the widths of the majority as well as minority spin states at the E_F along the Γ - K line in both $\text{Ni}_{0.90}\text{Fe}_{0.10}$ and $\text{Ni}_{0.80}\text{Fe}_{0.20}$. These re-

sults suggest that disorder scattering constitutes the main spin scattering mechanism in the Permalloys. The extent to which the KKR-CPA-LSD mean-field approach can provide a satisfactory description of spin scattering in magnetic materials more generally of course remains to be seen. In this connection, possible complications due to short-range ordering and clustering and other effects should also be kept in mind.¹⁰

Our computations yield considerable insight into the nature of the magnetic Ni and Fe potentials appropriate for the Permalloys. The majority spin KKR-CPA-LSD self-consistent potentials for the Ni and Fe sites in the alloy are found to be quite similar so that these electrons experience little disorder scattering. The minority spin potentials on the other hand are quite different, inducing large dampings of the minority spins in the system. These results are consistent with and provide a more quantitative basis for the model of two separate spin channels that has been invoked in the literature^{9,12,13} for explaining various properties of the Permalloys. We emphasize, however, that the effective disorder parameter in the alloy is quite complex and differs between *s-p* and *d* electrons, and depends strongly on the spin, symmetry, and the momentum of the specific states involved.

This article is organized as follows. Section II briefly addresses relevant computational aspects. The next section is divided into three subsections, the first of which discusses the nature of the spin-dependent Ni and Fe potentials and the associated effective disorder parameter in the Permalloys. Section III B discusses how the magnetic moments and the density of states on Ni and Fe sites and in various angular momentum channels evolve as a function of Fe concentration. The last subsection turns to the focal point of this paper which is to interpret the high-resolution ARPES spectra of Ref. 13 in terms of the spectral densities computed within the KKR-CPA-LSD framework. This discussion is divided into two subsections the first of which deals with the nature of the computed spectral density function and its relationship to the ARPES spectra. The other subsection then takes up a direct comparison of the relevant theoretical and experimental results. Section IV summarizes the conclusions of this work.

II. COMPUTATIONS

The electronic structure of $\text{Ni}_{1-x}\text{Fe}_x$ was computed semi-relativistically within the all-electron fully charge and spin self-consistent KKR-CPA framework for $x=0, 0.10, 0.20,$ and 0.50 . The results are parameter free except that the lattice constants were not determined via an energy minimization procedure; the specific concentration-dependent values used are listed in Table I.^{20,21} The underlying KKR-CPA methodology is described in Refs. 14–18. Exchange and correlation effects were incorporated within the von Barth–Hedin LSD approximation.^{22,23} The self-consistency cycles were repeated for each alloy composition until the maximum difference between the input and output muffin-tin potentials was less than 1 mRy at any mesh point in the unit cell. All calculations employ a maximum angular momentum cutoff $l_{max}=2$. The KKR-CPA cycles were carried out in the complex energy plane using a 48-point elliptic contour beginning

TABLE I. Room-temperature lattice constants used in the present computations for various compositions of $\text{Ni}_{1-x}\text{Fe}_x$ (in atomic units).

$x=0$	$x=0.10$	$x=0.20$	$x=0.50$
6.6579 ^a	6.6814 ^b	6.7049 ^c	6.7776 ^c

^aRef. 20.

^bBy linear interpolation between $x=0$ and $x=0.20$.

^cRef. 21.

at the bottom of the valence bands and ending at the Fermi energy which was determined to an accuracy of better than 0.1 mRy via the generalized Lloyd formula.¹⁶ The KKR-CPA Green function was computed on a 1330-special- \mathbf{k} -point mesh²⁴ (1540 special \mathbf{k} points for $x=0$) in the irreducible part of the BZ for each of the energy points in order to evaluate the integral over the BZ. In this way the KKR-CPA self-consistency condition was solved at each of the 48 basic energy points to an accuracy of about 1 part in 10^5 , followed by the computation of a new spin-dependent crystal potential. The starting potential for the next cycle was typically obtained by a roughly 1%–5% admixture of the new potential. The solution of the KKR-CPA condition required 1–10 iterations, while 100–200 charge and spin self-consistency cycles were usually needed depending on the alloy composition to achieve a high level of convergence (absolute accuracy of about 1 mRy) of the crystal potential. For the final potentials, the total density of states (DOS), site-decomposed component densities of states (CDOS), and the angular momentum (*l*) decomposed partial densities of states (PDOS) were computed on a 401-energy-point mesh using a tetrahedral \mathbf{k} -space integration technique²⁵ (with division of the 1/48th of the BZ into 17 496 small tetrahedra) applicable to ordered as well as disordered systems.

Finally, we note that the spectral density in the alloy (at momentum \mathbf{p} and energy E) is given by $A(\mathbf{p}, E) = -1/\pi \text{Im}\langle G(\mathbf{p}, \mathbf{p}) \rangle$ where $\langle G(\mathbf{p}, \mathbf{p}) \rangle$ is the momentum matrix element of the average Green function.¹⁹ For making contact with the ARPES experiments discussed in this article, however, the so-called Bloch spectral density $A_B(\mathbf{k}, E)$, which is obtained by folding $A(\mathbf{p}, E)$ into the first BZ, is more appropriate,^{26,27} $A(\mathbf{p}, E)$ enters more directly in the analysis of Compton scattering and positron-annihilation spectra.^{28,29} Accordingly, we present and discuss ARPES results on the 10% and 20% Fe Permalloys in Sec. III C below in terms of the spectral function $A_B(\mathbf{k}_{\parallel}, \mathbf{k}_{\perp}=\mathbf{0}, E_F)$.

III. RESULTS AND DISCUSSION

A. Nature of the spin-dependent Ni and Fe potentials in Permalloy and the associated effective “bands”

It is important first to understand the nature of the effective potentials associated with the Ni and Fe sites in the Permalloy. We emphasize that the standard crystal potentials used commonly for obtaining the magnetic band structures of fcc Ni or bcc Fe are not relevant here. In the alloy, the Ni and Fe atoms experience different surroundings, and in the case of Fe even the symmetry of the neighboring atoms is

different (fcc vs bcc). Moreover, interactions in the alloy lead in general to a redistribution of charge and spin states and to shifts in the positions of various levels. These fundamental effects of alloying are accounted for in the theory (at least in a mean-field sense) via the processes of charge, spin, and KKR-CPA self-consistency cycles. Therefore, the KKR-CPA self-consistent potentials for the Ni and Fe sites in $\text{Ni}_{1-x}\text{Fe}_x$ reflect the characteristics of these atoms in the alloy. Figure 1 shows effective majority and minority band structures for *hypothetical* fcc crystals of Ni and Fe using such final muffin-tin potentials in $\text{Ni}_{0.80}\text{Fe}_{0.20}$, and captures the essence of the behavior of the Ni and Fe atoms in the context of the Permalloys. Incidentally, we have carried out computations along these lines at other compositions (10% and 50% Fe)—the results are similar and are not shown in the interest of brevity. In short, the band structures of Fig. 1 provide a simple handle on the electronic structure of the Permalloys and we recall these results at several points in this article.^{30–32}

The relative positions of the Ni and Fe levels in the alloy can be read easily from Fig. 1 which allows one to obtain a sense of the effective disorder parameter at various \mathbf{k} points in the BZ. Figure 1(a) makes it clear that there is relatively little difference between the majority spin “bands” of Ni and Fe. Particularly the s - p bands and the upper portions of the d bands differ by no more than ~ 20 mRy. This implies that for the majority spin electrons there is a high degree of matching between the atomic potentials⁹ of Ni and Fe (i.e., one is in the virtual crystal regime^{32,33}) and therefore majority spin electrons will be expected to experience little scattering in the alloy.

The situation is markedly different for the minority spin electrons in Fig. 1(b). Here, the exchange splitting of the Fe bands is about 3 times larger than that of the Ni bands, resulting in the Fe minority spin d bands lying ~ 100 mRy above their Ni counterparts while for the s - p band the splitting is somewhat smaller (~ 60 mRy). A split-band model would more appropriately describe the minority d electrons.^{32,33} The stronger scattering potential will of course yield shorter scattering lengths for the minority spins. Note that the effective disorder parameter $\delta \sim \Delta/W$ where Δ is the difference between the levels of the two constituents while W is the relevant bandwidth.³³ Therefore, δ is substantially smaller for the minority s - p electrons compared to the d electrons since the s - p electrons not only possess a smaller Δ , but also involve a larger W . Figure 1 makes it clear that in general δ varies strongly with the spin, momentum, energy, and the symmetry of the states involved.

B. Evolution of magnetic moments and density of states

Insight into the evolution of the electronic structure of Permalloy is obtained from a consideration of the site- and l -decomposed densities of states with composition. Figure 2 shows the l decomposed density of states (PDOS) at Ni and Fe sites in $\text{Ni}_{0.80}\text{Fe}_{0.20}$. We see a full, sharply structured majority spin d band for both Ni and Fe with E_F lying a short distance above the upper d -band edge. In contrast, the minority spin band is generally much smoother and shifted to a

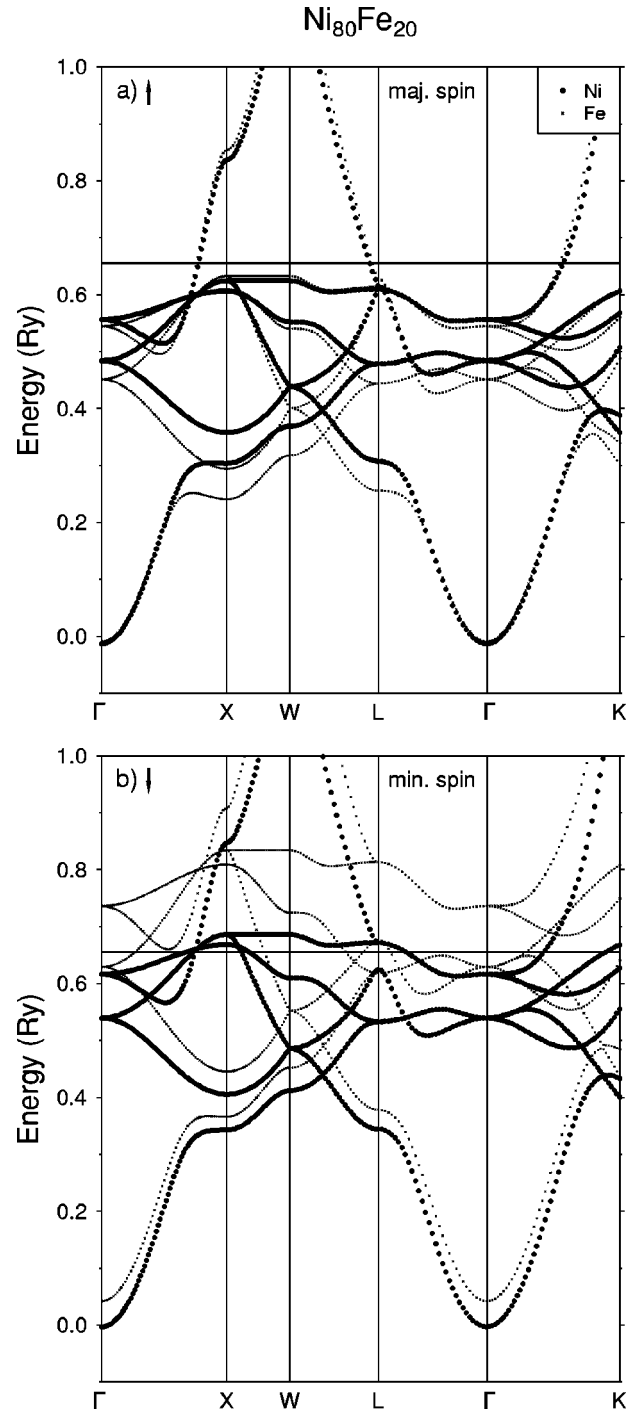


FIG. 1. Semirelativistic *hypothetical* band structures for majority and minority spin electrons obtained by placing the Ni (large dots) and Fe (small crosses) self-consistent KKR-CPA potentials in $\text{Ni}_{0.80}\text{Fe}_{0.20}$ on the alloy (fcc) lattice.

higher energy; the Fermi level intersects the Ni peak at the d -band edge, while the minority spin peak in Fe lies above E_F and is broadened owing to disorder scattering. The s and p electrons undergo little change upon alloying, display little exchange splitting, and possess a weight about 30 times smaller than the d states at E_F . For these reasons, the s - p electrons are essentially inert insofar as magnetic and disorder effects are concerned and will therefore be ignored from

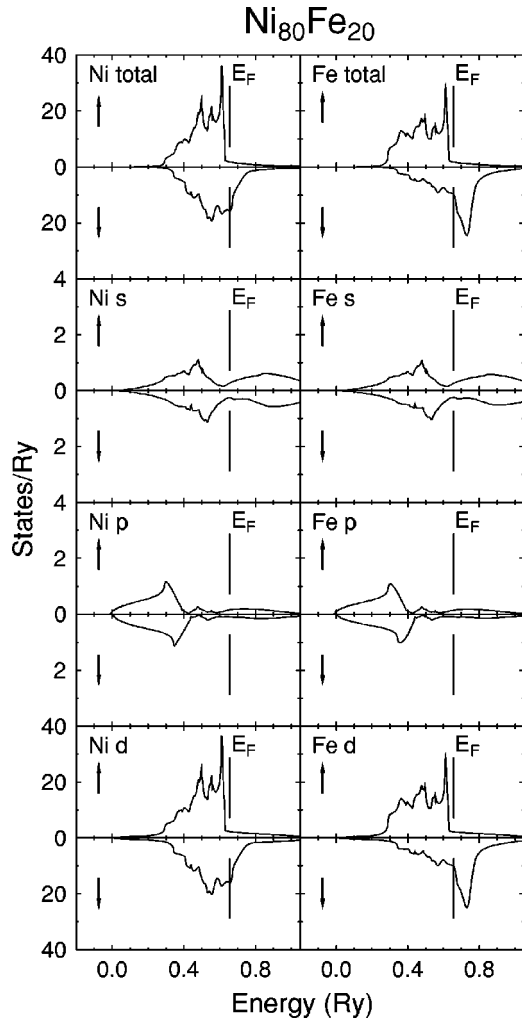


FIG. 2. Total densities of states associated with Ni and Fe sites in $\text{Ni}_{0.80}\text{Fe}_{0.20}$ are shown decomposed into angular momentum components (s , p , and d). The top half of each panel refers to the contribution from majority spins (\uparrow) and the bottom half to minority spins (\downarrow). Vertical lines mark the Fermi energy E_F . Note scale changes in different panels.

here onward in our discussion. The magnetic moment is carried mainly by the d electrons.

Figure 3 shows the evolution of the DOS at the Ni and Fe sites (CDOS) under alloying. Consistent with our earlier observations, the majority spin DOS on either site display little change in shape or structure with alloying. The changes in the minority DOS on the other hand are dramatic. In the single-impurity limit ($x=0$, right topmost panel), the Ni CDOS is of course that of pure Ni which is highly structured, while the Fe CDOS consists of a relatively sharp peak above the E_F —reminiscent of an impurity level—and a rather low but still quite structured DOS below E_F . The resulting uncompensated moment in the majority spin band induces a magnetic moment of $2.61\mu_B$ on the Fe impurity. As the Fe concentration increases, the disorder scattering of the minority spin electrons causes the structure in the DOS to be increasingly washed out until at $x=0.50$ a nearly structureless triangular looking DOS is left for Ni as well as for Fe.

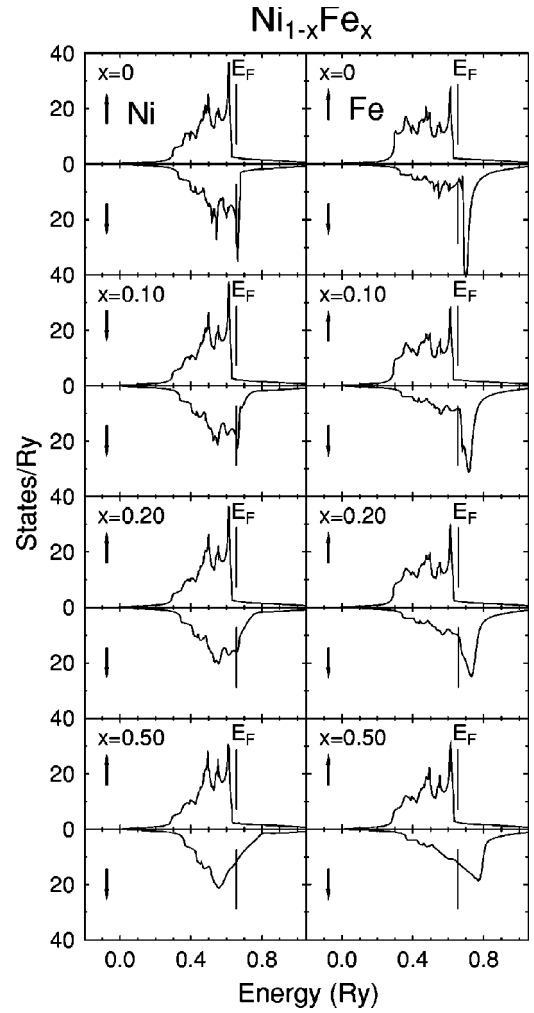


FIG. 3. Contributions from Ni and Fe sites to the total density of states in $\text{Ni}_{1-x}\text{Fe}_x$ are shown as a function of Fe concentration x . The top half of each panel refers to the majority spins (\uparrow) and the bottom half to minority spins (\downarrow). Vertical lines mark the Fermi energy E_F .

Some physical insight into the mechanism driving the preceding changes in moments and DOS may be obtained with the aid of the so-called “common band model” of bonding in d -band metals.^{34,35} Consider two atoms A and B with atomic energy level $E_A^0 < E_B^0$, which are assumed to broaden into bands of a common bandwidth W when the atoms are brought together to form a solid. From moment theory, it is known that the center of gravity of the local density of states (occupied and unoccupied) must coincide with the local on-site energy level $E_{A(B)}$ (which may be slightly shifted from the corresponding free-atom value in order to maintain local charge neutrality). We then obtain a new band of bandwidth W_{AB} , with transfer of charge from the B atom to the A atom until the Fermi levels line up. Owing to this redistribution, the states at the bottom of the band (the bonding states) become more concentrated on the A atom while the anti-bonding states at the top of the band are found preferentially on the B atom.

Applying this model to the minority bands of $\text{Ni}_{1-x}\text{Fe}_x$ where the atomic Ni $3d$ level lies lower in energy than the Fe

TABLE II. Computed magnetic moments (in μ_B) as a function of x in $\text{Ni}_{1-x}\text{Fe}_x$. The total (average) magnetic moment in the unit cell is decomposed into contributions from Fe and Ni muffin-tin spheres and from the interstitial region.

x	Fe	Ni	Interstitial	Total
0	2.61	0.65	-0.020	0.63
0.1	2.59	0.65	-0.019	0.82
0.2	2.57	0.65	-0.019	1.02
0.5	2.54	0.71	-0.020	1.61

$3d$ level (see Fig. 1), one expects a transfer of low-energy bonding charge from Fe to Ni as x increases, while the high-energy antibonding states move the other way from Ni to Fe. At first sight, the magnetic moments given in Table II seem to contradict this as the moments on both Fe and Ni are seen to remain essentially unchanged with increasing x (the negative s - p polarization in the interstitial region remaining more or less constant). The preceding argument, however, does not take into account the effect of disorder smearing of states which increases strongly with x for minority spins and complicates the situation. When states are broadened, some of the weight of the minority spins on Fe is spread from above to below E_F while the reverse happens with the minority spins on Ni with weight moving from below to above E_F . This effect tends to reduce the net Fe moment and to increase the Ni moment. Interestingly, the difference between the Fe and Ni moments is quite close to $2\mu_B$ —decreasing from $1.96\mu_B$ to $1.83\mu_B$ as we go from $x=0$ to $x=0.5$. Thus, the depletion of the electron system when a Ni atom is replaced by an Fe atom initially takes place almost entirely at the expense of the minority spin d band of Fe since the number of majority electrons for Ni and Fe remains practically the same.

C. Spectral density function and interpretation of angle-resolved photoemission spectra of Permalloys

1. Nature of spectral density function $A_B(\mathbf{k}_{\parallel}, \mathbf{k}_{\perp}=\mathbf{0}, E_F)$ along Γ - K

Before discussing the ARPES experiments of Ref. 13, we describe the character of $A_B(\mathbf{k}_{\parallel}, \mathbf{k}_{\perp}=\mathbf{0}, E_F)$ [from here onward this is denoted by $A_B(\mathbf{k}_{\parallel}, E_F)$ for simplicity of notation] (Ref. 36) in $\text{Ni}_{0.90}\text{Fe}_{0.10}$ and $\text{Ni}_{0.80}\text{Fe}_{0.20}$ with the help of Fig. 4. Note that the ARPES measurements of Ref. 13 were designed to investigate the nature of spin-resolved states at the Fermi level as one moves along the Γ - K direction in the BZ. This was accomplished by arranging the experimental parameters of photon energy and the momentum and energy of the emitted electrons appropriately. Our theoretical analysis is based on the computed spectral density $A_B(\mathbf{k}_{\parallel}, E_F)$ as a function of \mathbf{k}_{\parallel} along $[011]$ with E fixed at E_F and reproduces the experimental conditions of energy and momentum of the initial states correctly. On the other hand, matrix element effects in the ARPES spectrum³⁷ are not described properly by $A_B(\mathbf{k}_{\parallel}, E_F)$; these effects in general alter the intensities of peaks in $A_B(\mathbf{k}_{\parallel}, E_F)$ and in some cases suppress specific

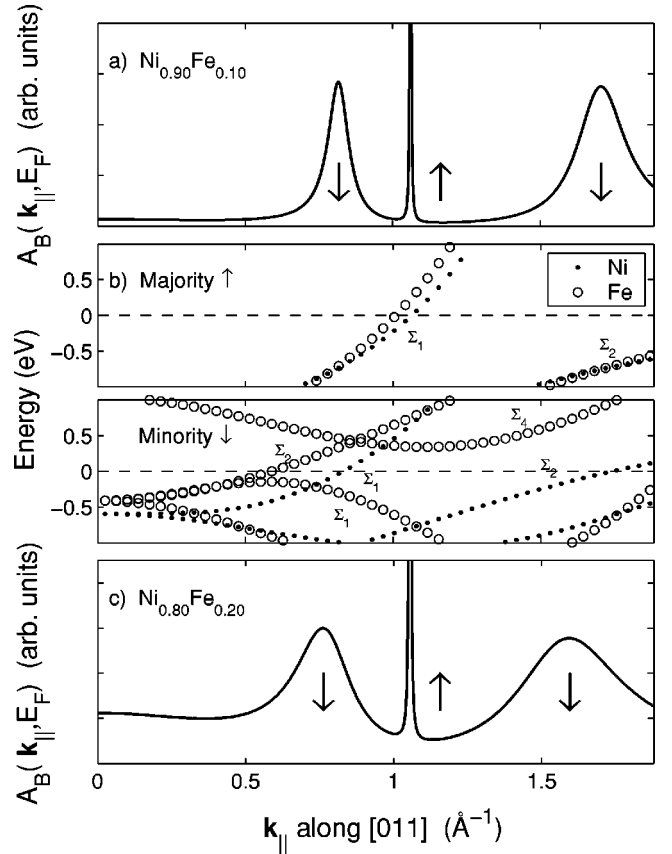


FIG. 4. Computed spectral density function $A_B(\mathbf{k}_{\parallel}, \mathbf{k}_{\perp}=\mathbf{0}, E_F)$ in $\text{Ni}_{0.90}\text{Fe}_{0.10}$ and $\text{Ni}_{0.80}\text{Fe}_{0.20}$ when E is fixed at the Fermi energy E_F and $|\mathbf{k}_{\parallel}|$ is varied along the $[011]$ direction in the BZ. The arrows refer to majority (\uparrow) and minority (\downarrow) spin peaks discussed in the text. Two panels in the middle (b) show a blowup of the effective Ni (solid circles) and Fe (open circles) bands of Fig. 1 along the Γ - K direction in the vicinity of E_F (shown by the dashed line); the symmetry labels of various bands around E_F are marked (Ref. 39).

transitions altogether via selection rules. Nevertheless, we expect the positions and widths of the peaks in the ARPES spectra to be given reasonably well by $A_B(\mathbf{k}_{\parallel}, E_F)$ for our purpose of understanding the spin-dependent disorder scattering in the alloy, effects of selection rules notwithstanding.³⁸

Figure 4 shows the theoretical spectral density $A_B(\mathbf{k}_{\parallel}, E_F)$ along $[011]$ for $|\mathbf{k}_{\parallel}|$ values over the range $0-1.9 \text{ \AA}^{-1}$. Considering Fig. 4(a) for $\text{Ni}_{0.90}\text{Fe}_{0.10}$ first, we see three peaks. The central peak at 1.062 \AA^{-1} is very sharp and is related to the states in the alloy arising from the effective majority spin Σ_1 bands for Ni and Fe of Fig. 1, which coalesce into a single peak in the alloy [the relevant parts of Fig. 1 are reproduced in Fig. 4(b) for convenient reference].³⁹ On either side of this up-spin Σ_1 peak, there are broad peaks at 0.816 \AA^{-1} [full width at half maximum (FWHM) = 0.08 \AA^{-1}] and 1.706 \AA^{-1} (FWHM = 0.20 \AA^{-1}). Comparison with the band structures of Fig. 4(b) reveals that the leftmost of the peaks should be ascribed to the states originating in the alloy mainly from the minority spin Ni Σ_1 band which intersects the Fermi level; similarly, the peak on

the right arises primarily from the minority spin Σ_2 band of Ni. We emphasize that the precise positions of the peaks in Fig. 4(a) do not (and need not) match the \mathbf{k}_{\parallel} points of intersection of specific bands (at E_F) involved because these states will interact and mix and will thus be modified to yield the alloy spectrum.

Figure 4(c) considers similar results for the spectral density function at E_F for $\text{Ni}_{0.80}\text{Fe}_{0.20}$. Again, three peaks are found of which the central one (at 1.056 \AA^{-1}) is due to the majority spins, while the two others (at 0.762 \AA^{-1} and 1.594 \AA^{-1}) are from minority spins. Some of the preceding discussion of Fig. 4(a) for $\text{Ni}_{0.90}\text{Fe}_{0.10}$ is applicable here and need not be repeated. Interestingly, comparing the lower minority peak at $|\mathbf{k}_{\parallel}| \approx 0.8 \text{ \AA}^{-1}$ in Figs. 4(a) and 4(c), the effect of the Fe impurities is more apparent; the line shape of this feature is more skewed in Fig. 4(c) as the spectral weight of the Fe states grows in the 20% alloy. Despite the fact that every state in the alloy involves a mixture of Ni and Fe states, the central peak is dominated by majority spin Ni Σ_1 electrons, although these are in a practical sense quite indistinguishable from majority spin Fe Σ_1 electrons. On the other hand, the lower minority spin peak in Figs. 4(a) and 4(c) contains contributions from Ni Σ_1 and Fe Σ_2 electrons which are separated in \mathbf{k}_{\parallel} , but because the Fe part is quite broad and possesses relatively small weight, the net effect is to cause the aforementioned skewing of the peak rather than the appearance of a distinct additional peak in the spectral density. In this vein, the right-hand peak is largely composed of Ni Σ_2 minority states with some background contribution from tails of other nearby levels as they are broadened upon alloying.

Consistent with our earlier observations, Fig. 4 immediately makes it clear that the majority electrons of Ni (giving rise to the central peak) see little disorder scattering when Fe impurities are added, while the minority spins experience quite large damping. In connection with the widths of the peaks in $A_B(\mathbf{k}_{\parallel}, E)$, it is important to note that $A_B(\mathbf{k}_{\parallel}, E)$ can be displayed as a function of $|\mathbf{k}_{\parallel}|$ with E fixed or, alternatively, as a function of E with $|\mathbf{k}_{\parallel}|$ fixed. In either case the finite peak widths reflect the disorder-induced smearing of states and thus possess the same physical origin. However, the peak width δk (for fixed E) is related to the corresponding width δE (when \mathbf{k} is held fixed) via $\delta k \sim \delta E/v_k$ where $v_k = \partial E/\partial k$ is the appropriate group velocity. These effects are properly accounted for in the theory in obtaining the results of Fig. 4.

2. Comparison with high-resolution ARPES spectra

We are in a position now to make direct contact with the ARPES spectra from $\text{Ni}_{0.90}\text{Fe}_{0.10}$ and $\text{Ni}_{0.80}\text{Fe}_{0.20}$ with reference to Fig. 5 and Table III. For this purpose, Fig. 5 shows the spectral functions of Fig. 4 except that these have now been broadened to reflect experimental resolution; moreover, the data are plotted over the momentum range of $0.6\text{--}1.3 \text{ \AA}^{-1}$ over which the experimental spectra of Ref. 13 were measured. The upper (minority) peak of Figs. 4(a) and 4(c) is thus not shown in Fig. 5. We have, however, done so purposely since in the experimental geometry employed

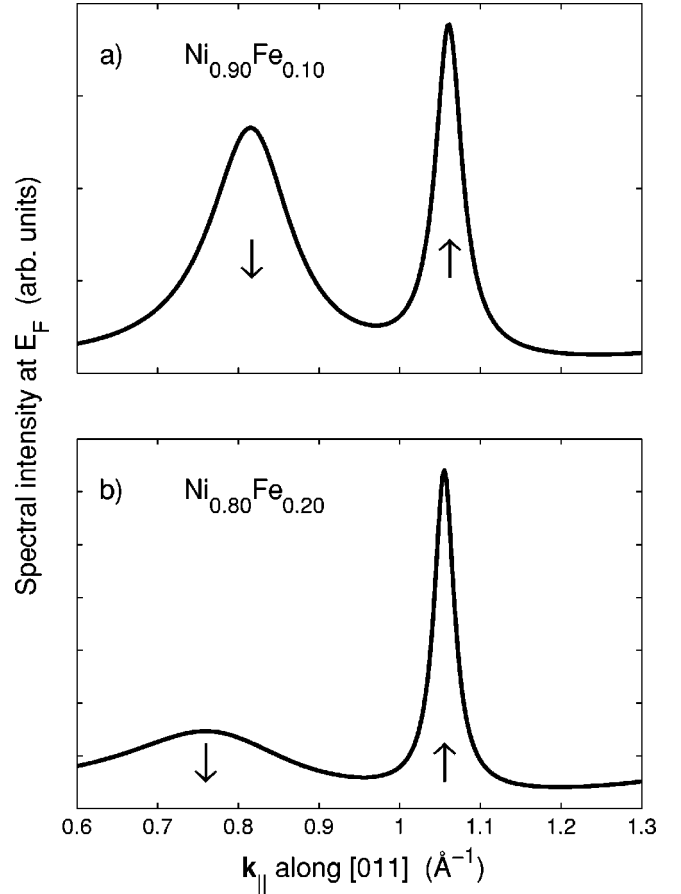


FIG. 5. Theoretical spectral intensities in $\text{Ni}_{0.90}\text{Fe}_{0.10}$ and $\text{Ni}_{0.80}\text{Fe}_{0.20}$ for emission from E_F as \mathbf{k}_{\parallel} is varied along the [011] direction over a \mathbf{k}_{\parallel} range appropriate for analyzing the ARPES spectra of Ref. 13. The spectra have been broadened to reflect experimental resolution. Arrows identify features arising from majority (\uparrow) and minority (\downarrow) spin electrons.

by Ref. 13, selection rules only allow transitions from initial states of Σ_1 symmetry. Transitions from other initial states such as Σ_2 or Σ_4 are forbidden.⁴⁰ Notably, an examination of the shape of the *experimental* ARPES peaks, especially of the majority spin peak which in view of its significant *s-p* character and ensuing small δ is resolution limited, indicates that these peaks are reasonably well described by a Lorentzian. Accordingly, the results of Fig. 5 involve a convolution with a Lorentzian resolution function of FWHM $= 0.0380 \text{ \AA}^{-1}$ for the 10% alloy and of FWHM $= 0.0285 \text{ \AA}^{-1}$ for the 20% alloy.⁴¹

Table III collects the positions and widths of the majority and minority spin peaks in Fig. 5, together with the corresponding experimental values from the ARPES data of Ref. 13. The agreement between theory and experiment with respect to the widths of peaks is remarkably good in all cases. The fact that the experimental majority peak is resolution limited indicates that the majority spin electrons see little disorder scattering as predicted theoretically. For the minority electrons, the computed widths of 0.12 \AA^{-1} and 0.22 \AA^{-1} for the 10% and 20% Fe, respectively, are in excellent accord with the experimental widths of 0.10 \AA^{-1}

TABLE III. Theoretical majority (k_{\uparrow}) and minority (k_{\downarrow}) spin peak positions and widths $\delta k_{\uparrow(\downarrow)}$ (FWHM) in $\text{Ni}_{1-x}\text{Fe}_x$ based on the theoretical data of Fig. 5 are compared with the corresponding experimental values taken from Ref. 13. The exchange splittings $\Delta k_{\text{exch}} \equiv k_{\uparrow} - k_{\downarrow}$ are listed. Theoretical results have been broadened to reflect experimental resolution. All entries are in \AA^{-1} units.

x	Theory					Experiment				
	k_{\uparrow}	k_{\downarrow}	Δk_{exch}	δk_{\uparrow}	δk_{\downarrow}	k_{\uparrow}	k_{\downarrow}	Δk_{exch}	δk_{\uparrow}	δk_{\downarrow}
0.10	1.062	0.816	0.246	0.04	0.12	1.05	0.92	0.14	0.04	0.10
0.20	1.056	0.762	0.294	0.03	0.22	1.05	0.92	0.14	0.03	0.22

and 0.22 \AA^{-1} .⁴² These results leave little doubt that the observed lifetimes of the majority and minority spin electrons in the Ni-rich Permalloys can be explained quantitatively as a simple consequence of disorder scattering.

Insofar as the Fermi surface radii given by the peak positions (k_{\uparrow} and k_{\downarrow}) are concerned, we see from Table III that the measured k_{\uparrow} values are in reasonable accord with the theoretical values, although the slight predicted decrease in the radius from 1.062 \AA^{-1} to 1.056 \AA^{-1} to account for the depleted electron count in going from the 10% to the 20% concentration would be difficult to observe within the experimental resolution. On the other hand, the computed minority radii k_{\downarrow} are systematically smaller than the experimental values. As a result, the theoretical exchange splitting is larger than the measured values. This discrepancy is well known in Ni and reflects the inadequacy of the LSD in this regard. In this connection we have carried out a number of simulations in which the size of the exchange splitting in Ni was varied by changing the minority potential in an *ad hoc* manner. The widths of the peaks in the spectral function were, however, found to be insensitive to such variations, indicating that the theoretical results of Table III are robust in this regard.

IV. SUMMARY AND CONCLUSIONS

We have carried out fully charge and spin self-consistent all-electron KKR-CPA-LSD computations in $\text{Ni}_{1-x}\text{Fe}_x$ disordered alloys for $x=0.10, 0.20, 0.50$ and the case of a single Fe impurity in Ni (i.e., $x=0$). Otherwise, the results are parameter free except that the lattice constants were not obtained by minimizing the total energy. Recent high-resolution ARPES experiments of Ref. 13 on $\text{Ni}_{0.90}\text{Fe}_{0.10}$ and $\text{Ni}_{0.80}\text{Fe}_{0.20}$ Permalloys are analyzed in some detail. For this purpose, the spectral density function $A_B(\mathbf{k}_{\parallel}, \mathbf{k}_{\perp}=\mathbf{0}, E_F)$ is computed in the alloys from the KKR-CPA Green function for $|\mathbf{k}_{\parallel}|$ values varying along the Γ - K direction in the BZ in order to properly describe the geometrical setup of the ARPES experiments. The widths of the majority as well as the minority spin peaks in the theoretical spectra are in excellent accord with the corresponding widths of the ARPES peaks in both the 10% and the 20% Fe alloy. This suggests that spin-dependent disorder scattering constitutes the main scattering mechanism for the carriers in the Permalloys and that this physics is captured reasonably well by the present

theoretical framework. Majority spin states of Ni are virtually undamped by Fe impurities, while the minority spins at the Fermi level are heavily damped.

The nature of the Ni and Fe potentials in the Permalloys is explored in detail. For the majority spins the Ni and Fe potentials are nearly the same, while for the minority spins the two potentials differ greatly. In this connection, a set of effective magnetic energy bands is computed by placing the self-consistent KKR-CPA potentials for Ni and Fe in the alloy on a hypothetical fcc lattice. These ‘‘bands’’ yield considerable insight into the behavior of the alloy spectrum by allowing an easy visualization of the effective disorder parameter δ , whose values differ greatly for the minority spins at different \mathbf{k}_{\parallel} points in the BZ and, even at a given \mathbf{k} point, δ depends strongly on the spin and symmetry of the states involved. We describe the evolution of the electronic states and magnetic moments on the Ni and Fe sites as a function of Fe concentration. The majority spin densities of states are essentially unchanged upon alloying, but the minority spin densities undergo substantial changes and display considerable broadening in the alloy. The magnetic moment on Fe as well as Ni sites remains essentially unchanged with increasing Fe content as a result of an interplay between the movements of spectral weights of bonding and antibonding states on the one hand and the effect of broadening of minority levels in the alloy due to disorder scattering on the other. Further ARPES studies of magnetic alloys along these lines would prove worthwhile for establishing not only the range of validity of the present KKR-CPA-LSD approach but also for clarifying the nature of the disorder parameter in various interesting cases.

ACKNOWLEDGMENTS

It is a pleasure to acknowledge important conversations with Franz Himpsel who suggested that we look into the spin-resolved electronic structure of Permalloy in view of recent advances in ARPES studies of magnetic materials. This work is supported by U.S. Department of Energy Contract No. W-31-109-ENG-38 and benefited from the allocation of supercomputer time at the NERSC and the Northeastern University Advanced Scientific Computation Center (ASCC). One of us (S.S.) acknowledges Suomen Akatemia, Vilho, Yrjö ja Kalle Väisälän Rahasto, Tekniikan Edistämissäätiö, and Jenny ja Antti Wihurin Rahasto for financial support.

- ¹See, e.g., F.J. Himpsel, J.E. Ortega, G.J. Mankey, and R.F. Willis, *Adv. Phys.* **47**, 511 (1998).
- ²B. Diény, V.S. Speriosu, S.S.P. Parkin, B.A. Gurney, D.R. Wilhoit, and D. Mauri, *Phys. Rev. B* **43**, 1297 (1991).
- ³C. Tsang, R.E. Fontana, T. Lin, D.E. Heim, V.S. Speriosu, B.A. Gurney, and M. Williams, *IEEE Trans. Magn.* **MAG-30**, 3801 (1994).
- ⁴B.A. Gurney, V.S. Speriosu, J.P. Nozieres, H. Lefakis, D.R. Wilhoit, and O.U. Need, *Phys. Rev. Lett.* **71**, 4023 (1993).
- ⁵B. Diény, *Europhys. Lett.* **17**, 261 (1992).
- ⁶A. Barthelemy and A. Fert, *Phys. Rev. B* **43**, 13 124 (1991).
- ⁷P. Levy, S. Zhang, and A. Fert, *Phys. Rev. Lett.* **65**, 1643 (1990).
- ⁸B.L. Johnson and R.E. Camley, *Phys. Rev. B* **44**, 9997 (1991).
- ⁹W.H. Butler, X.-G. Zhang, D.M.C. Nicholson, and J.M. MacLaren, *J. Magn. Magn. Mater.* **151**, 354 (1995).
- ¹⁰D.M.C. Nicholson, W.H. Butler, W.A. Shelton, Y. Wang, X.-G. Zhang, G.M. Stocks, and J.M. MacLaren, *J. Appl. Phys.* **81**, 4023 (1997).
- ¹¹J.M. MacLaren, X.-G. Zhang, and W.H. Butler, *Phys. Rev. B* **56**, 11 827 (1997).
- ¹²F.J. Himpsel, K.N. Altmann, G.J. Mankey, J.E. Ortega, and D.Y. Petrovykh, *J. Magn. Magn. Mater.* **200**, 456 (1999).
- ¹³D.Y. Petrovykh, K.N. Altmann, H. Höchst, M. Laubscher, S. Maat, G.J. Mankey, and F.J. Himpsel, *Appl. Phys. Lett.* **73**, 3459 (1998); K.N. Altmann, N. Gilman, J. Hayoz, R.F. Willis, and F.J. Himpsel, *Phys. Rev. Lett.* **87**, 137201-1 (2001).
- ¹⁴A. Bansil, S. Kaprzyk, P.E. Mijnaerends, and J. Toboła, *Phys. Rev. B* **60**, 13 396 (1999).
- ¹⁵A. Bansil, S. Kaprzyk, and J. Toboła, in *Applications of Multiple Scattering Theory to Materials Science*, edited by W.H. Butler, P.H. Dederichs, A. Gonis, and R. Weaver, *Mater. Res. Soc. Symp. Proc. No. 253* (Materials Research Society, Pittsburgh, 1992), p. 505.
- ¹⁶S. Kaprzyk and A. Bansil, *Phys. Rev. B* **42**, 7358 (1990).
- ¹⁷A. Bansil and S. Kaprzyk, *Phys. Rev. B* **43**, 10 335 (1991).
- ¹⁸S. Kaprzyk, *Acta Phys. Pol. A* **91**, 135 (1997).
- ¹⁹A. Bansil, R.S. Rao, P.E. Mijnaerends, and L. Schwartz, *Phys. Rev. B* **23**, 3608 (1981).
- ²⁰P. Villars and L.D. Calvert, *Pearson's Handbook of Crystallographic Data for Intermetallic Phases* (American Society of Metals, Metals Park, OH, 1985), Vol. 3.
- ²¹R.J. Wakelin and E.L. Yates, *Proc. Phys. Soc. London, Sect. B* **66**, 221 (1953).
- ²²U. von Barth and L. Hedin, *J. Phys. C* **5**, 1629 (1972); A.K. Rajagopal and J. Callaway, *Phys. Rev. B* **7**, 1912 (1973).
- ²³Other, perhaps more satisfactory forms of the exchange-correlation functional could of course be used in the process of obtaining the self-consistent crystal potential. However, such differences are not particularly significant within the context of this article.
- ²⁴S. Froyen, *Phys. Rev. B* **39**, 3168 (1989).
- ²⁵S. Kaprzyk and P.E. Mijnaerends, *J. Phys. C* **19**, 1283 (1986).
- ²⁶P.E. Mijnaerends and A. Bansil, *Phys. Rev. B* **13**, 2381 (1976).
- ²⁷ $A_B(\mathbf{k}, E)$ allows a clearer identification of various spectral features for the \mathbf{k}_\parallel values which lie in the first BZ and are of interest in this article. For a given crystal momentum \mathbf{k} , $A(\mathbf{p}, E)$ in general contains peaks at various momenta $\mathbf{k} + \mathbf{K}$ where \mathbf{K} denotes a reciprocal lattice vector. The spectral weights in either $A(\mathbf{p}, E)$ or $A_B(\mathbf{k}, E)$ are not representative of the ARPES spectra since these weights will be modified by the ARPES matrix element which is not included in our computations.
- ²⁸A. Bansil, *Z. Naturforsch., A: Phys. Sci.* **48**, 165 (1993).
- ²⁹P.E. Mijnaerends and A. Bansil, in *Positron Spectroscopy of Solids*, edited by A. Dupasquier and A.P. Mills (IOS Press, Amsterdam, 1995), p. 25.
- ³⁰A more sophisticated description is provided by the so-called complex energy bands (see Refs. 31 and 32) which encode the positions and disorder-induced widths (but not the weights) of the spectral peaks in the alloy.
- ³¹A. Bansil, H. Ehrenreich, L. Schwartz, and R.E. Watson, *Phys. Rev. B* **9**, 445 (1974).
- ³²A. Bansil, in *Positron Annihilation*, edited by P.G. Coleman, S.G. Sharma, and L.M. Diana (North-Holland, Amsterdam, 1982), p. 291.
- ³³See, e.g., H. Ehrenreich and L. Schwartz, *Solid State Phys.* **31**, 149 (1976).
- ³⁴D.G. Pettifor, *Bonding and Structure of Molecules and Solids* (Clarendon, Oxford, 1995), p. 191.
- ³⁵A.R. Williams, V.L. Moruzzi, C.D. Gelatt, J. Kübler, and K. Schwartz, *J. Appl. Phys.* **53**, 2019 (1982).
- ³⁶It should be noted that in the experimental spectra of Ref. 13 being analyzed here, \mathbf{k}_\perp is approximately, but not strictly, zero.
- ³⁷A. Bansil and M. Lindroos, *Phys. Rev. Lett.* **83**, 5154 (1999).
- ³⁸Of course, the line shape can also be influenced if the ARPES matrix element is strongly energy and/or momentum dependent.
- ³⁹As already noted, although the effective bands of Figs. 1 and 4(b) refer to $\text{Ni}_{0.80}\text{Fe}_{0.20}$, these are relevant for discussing Ni-rich NiFe alloys more generally.
- ⁴⁰Bearing in mind our remarks on this point in the preceding Sec. III C 1, the upper feature of symmetry Σ_2 in the spectral function of Figs. 4(a) and 4(c) will be suppressed in the ARPES spectra and is thus irrelevant in connection with the present comparisons. The extent to which the smearing of states in an alloy may compromise the strict constraints of selection rules is not clear; see, e.g., P.J. Durham, *J. Phys. F: Met. Phys.* **11**, 2475 (1981).
- ⁴¹In addition to the experimental momentum resolution of 0.01 \AA^{-1} , which is the same for both samples, the difference in broadening is caused by, e.g., sample imperfections and residual \mathbf{k}_\perp broadening (see Refs. 12 and 13).
- ⁴²Of course, the mean free path λ is found from the broadening δk via the uncertainty relation $\lambda = 1/\delta k$. Thus, the minority peak width $\delta k_\perp = 0.22 \text{ \AA}^{-1}$ for $\text{Ni}_{0.80}\text{Fe}_{0.20}$ would imply a mean free path of 4.5 \AA .